

# SoftGroup++: Scalable 3D Instance Segmentation with Octree Pyramid Grouping

Thang Vu, Kookhoi Kim, Tung M. Luu, Thanh Nguyen, Junyeong Kim, Chang D. Yoo  
Department of Electrical Engineering  
Korea Advanced Institute of Science and Technology

## Abstract

Existing state-of-the-art 3D point cloud instance segmentation methods rely on a grouping-based approach that groups points to obtain object instances. Despite improvement in producing accurate segmentation results, these methods lack scalability and commonly require dividing large input into multiple parts. To process a scene with millions of points, the existing fastest method SoftGroup [37] requires tens of seconds, which is under satisfaction. Our finding is that  $k$ -Nearest Neighbor ( $k$ -NN), which serves as the prerequisite of grouping, is a computational bottleneck. This bottleneck severely worsens the inference time in the scene with a large number of points. This paper proposes SoftGroup++ to address this computational bottleneck and further optimize the inference speed of the whole network. SoftGroup++ is built upon SoftGroup, which differs in three important aspects: (1) performs octree  $k$ -NN instead of vanilla  $k$ -NN to reduce time complexity from  $\mathcal{O}(n^2)$  to  $\mathcal{O}(n \log n)$ , (2) performs pyramid scaling that adaptively downsamples backbone outputs to reduce search space for  $k$ -NN and grouping, and (3) performs late devoxelization that delays the conversion from voxels to points towards the end of the model such that intermediate components operate at a low computational cost. Extensive experiments on various indoor and outdoor datasets demonstrate the efficacy of the proposed SoftGroup++. Notably, SoftGroup++ processes large scenes of millions of points by a single forward without dividing the input into multiple parts, thus enriching contextual information. Especially, SoftGroup++ achieves 2.4 points AP<sub>50</sub> improvement while nearly  $6\times$  faster than the existing fastest method on S3DIS dataset. The code and trained models will be made publicly available.

## 1 Introduction

With the rapid development of 3D sensors and the availability of large-scale 3D datasets, instance segmentation on 3D point clouds has received considerable attention. Given input point clouds, instance segmentation detects objects of interest, each of which is assigned to a class label and a point-level instance mask. 3D instance segmentation has a wide range of applications in different areas, such as virtual reality [41, 47], autonomous driving [6], and robot navigation [14, 33].

Recent state-of-the-art methods have made great strides in improving the performance of the segmentation predictions [38, 39, 44, 21, 26, 13, 20, 37]. However, these methods still show limited scalability. We define scalability as the ability to maintain fast inference speed when the input size increases. Figure 1a shows that the runtimes of existing methods grow quickly as the number of points increases. For instance, existing methods requires from  $\sim 20$ s to  $\sim 50$ s to process a scene of  $\sim 4.5$ M points. The processing time of each network component for this scene is further analyzed, as provided Figure 1b. The results reveal that  $k$ -NN is the computational bottleneck, leading to the quick growth of inference time w.r.t. input size in HAIS [5] and SoftGroup [37]. This is because

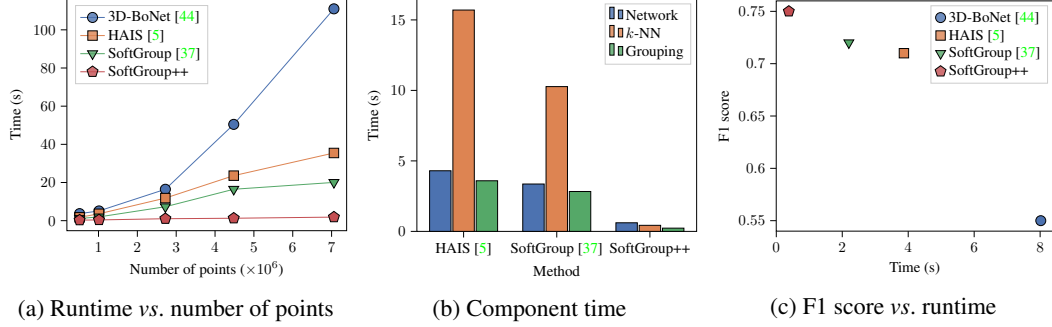


Figure 1: (a) **Runtime vs. number of points.** The runtimes of existing methods significantly increase as the number of points increases. (b) **Component time.** We measure the component time of processing a large scene of  $\sim 4.5$ M points. The measurement exposes  $k$ -NN as computational bottleneck of existing methods. (c) **F1 score vs. runtime.** We compare F1 score<sup>1</sup> vs. runtime between the proposed SoftGroup++ and existing methods on Area 5 of S3DIS dataset [1]. The results shows that our methods is faster and more accurate.

these methods perform vanilla  $k$ -NN that requires pair-wise distance measurement of the whole point set with time complexity of  $\mathcal{O}(n^2)$ , resulting in limited scalability.

This paper proposes an architecture referred to as SoftGroup++ for scalable 3D instance segmentation on point clouds with three important aspects. *First*, SoftGroup++ performs octree  $k$ -NN instead of vanilla  $k$ -NN to reduce time complexity from  $\mathcal{O}(n^2)$  to  $\mathcal{O}(n \log n)$ . To effectively parallelize octree  $k$ -NN on GPU, a strategy to unfold the recursive structure of octree is presented such that tree traversal can be derived from simple arithmetic. *Second*, SoftGroup++ performs pyramid scaling to adaptively downsample on the backbone outputs to reduce the search space for  $k$ -NN and grouping. *Third*, SoftGroup++ performs late devoxelization to delay the conversion from voxels to points until the end of the model such that intermediate network components operate at a lower computational cost. Figure 1a shows that our method still maintains fast inference speed as input size significantly increases. The computational bottleneck of  $k$ -NN is also addressed, as presented in Figure 1b. Since our model is efficient, it can process scenes with millions of points in a single forward without dividing the input into multiple parts, thus providing better contextual information. As illustrated in Figure 1c, our method is not only faster but also more accurate than the others. In summary, our contributions are threefold.

- We investigate the scalability of recent 3D instance segmentation methods and reveal the computational bottleneck of  $k$ -NN.
- We propose SoftGroup++ for scalable 3D instance segmentation through three components: octree  $k$ -NN, pyramid scaling, and late devoxelization. Octree  $k$ -NN reduces the time complexity of  $k$ -NN, while pyramid scaling and late devoxelization reduce the search space and runtime of intermediate network components.
- We report extensive experiments on various datasets with significant improvements in terms of average precision and inference speed, demonstrating the superiority and generality of our method.

## 2 Related Work

**3D Deep Learning on Point Clouds.** Point cloud representation is a common data format for 3D scene understanding. In contrast to 2D images, 3D point clouds are sparse and unstructured, causing extra difficulties in feature extraction. Early methods extracts hand-crafted features based on statistical properties of points [2, 31, 32, 3]. Recent deep learning methods learn to extract point features. PointNet-based methods [27, 28] propose to process points through shared Multi-Layer Perceptron (MLP) and then aggregate regional and global features from symmetric function, such as

<sup>1</sup>The scores of some methods are only available in terms of precision and recall. We use F1 score as the single performance indicator to ease the visualization.



max-pooling. Convolution methods are actively explored for point clouds processing. Continuous convolution methods [43, 22, 42, 36] learn the kernels which are associated to the spatial distribution of local points. Discrete convolution methods [12, 19, 9, 7, 24, 29] learn the kernels which are regular grids obtaining from point quantization. Transformers [18, 46, 17] and graph-based methods [35, 34, 40] are also widely explored for 3D scene understanding.

**3D Instance Segmentation.** 3D instance segmentation can be roughly categorized into proposal-based and grouping-based methods. Proposal-based methods generate region proposals and then segment the object within each proposal. GSPN [45] takes an analysis-by-synthesis strategy for generating proposals, reconstructing shapes from noisy observations in a scene to leverage geometric understanding. 3DSIS [11] jointly learns geometric and color information with multi-view RGB-D images to predict bounding boxes and object instances. 3D-BoNet [44] directly regresses 3D bounding boxes in a single stage without the utilization of anchors and any post-processing such as non-maximum suppression, followed by predicting point masks for instance segmentation. GICN [21] predicts Gaussian center heatmaps that characterize the instance centers and then selects center candidates to generate bounding boxes and instance masks.

Grouping-based methods first predict the point-wise labels (such as semantic maps, geometric offsets, or latent features) and then use clustering methods to generate instance predictions. SGPN [38] constructs a feature similarity matrix for all points and then group points of similar features into instances. JSIS3D [26] is a unified framework to jointly optimize point-wise semantic and instance predictions with a multi-value conditional random field. MTML [16] learning feature and directional embedding and then group instances with mean-shift clustering. OccuSeg [10] introduces graph-based grouping guided by object occupancy signal. PointGroup [13] groups nearby points of the same label and expands the group progressively. HAIS [5] extends PointGroup to aggregate fragment proposals with the corresponding primary instance and aggregated proposals are then refined by an intra-instance prediction network. SSTNet [20] constructs a semantic superpoint tree that is traversed and split at intermediate nodes to obtain object instances. SoftGroup [37] proposes to perform grouping on soft semantic scores to address the problem of the hard semantic predictions that propagates the errors to instance predictions. Despite improvements in accurateness, these methods are generally slow to handle large scenes. We propose a novel framework with a low computational cost to handle large scenes efficiently.

**Divide-and-Merge Strategy.** Divide-and-merge is the strategy to divide input into multiple parts and then merge the predictions of these parts to obtain final results. This strategy is widely adopted in processing large 3D scenes in existing 3D instance segmentation methods. In [38, 39, 44, 21, 26], the point cloud input is divided into overlapping blocks (*e.g.*,  $1\text{m} \times 1\text{m}$ ), and perform subsample within each block with a fixed number of points (*e.g.*, 4096). Then, the segmentation results from different blocks are merged using the BlockMerging algorithm [38]. In [13, 20, 37], large scenes are divided into 4 parts, and then the predictions are merged to obtain the final results. The divide-and-merge strategy exhibits various drawbacks. It limits the contextual information since the parts are processed independently. It needs to deal with point predictions in junction areas and requires extra post-processing time. Our method processes large scenes in a single forward without dividing them into multiple parts, thus avoiding the limitations of divide-and-merge strategy.

### 3 Method

Before delving into the proposed SoftGroup++, we revisit its predecessor SoftGroup [37]. As illustrated in Figure 2a, the input point clouds are voxelized before being fed into a U-Net style backbone [30]. Then the backbone features are devoxelized to obtain point-level features, which are used to learn semantic and offset predictions. Based on the semantic and offset predictions, a vanilla  $k$ -NN constructs the adjacency matrix of all points. Then a soft grouping module traverses through the graph represented by the adjacency matrix to group points of similar semantic predictions with close distances into instance proposals. These proposals are further refined to get the final instances.

As shown in Figure 2b, the proposed SoftGroup++ differs from SoftGroup in three aspects: (1) an octree  $k$ -NN is proposed to address the bottleneck stemming from vanilla  $k$ -NN, (2) a pyramid scaling is proposed to reduce the search space of  $k$ -NN and grouping, and (3) devoxelization is performed at the end of the network such that all intermediate components run at a low computational cost. In the

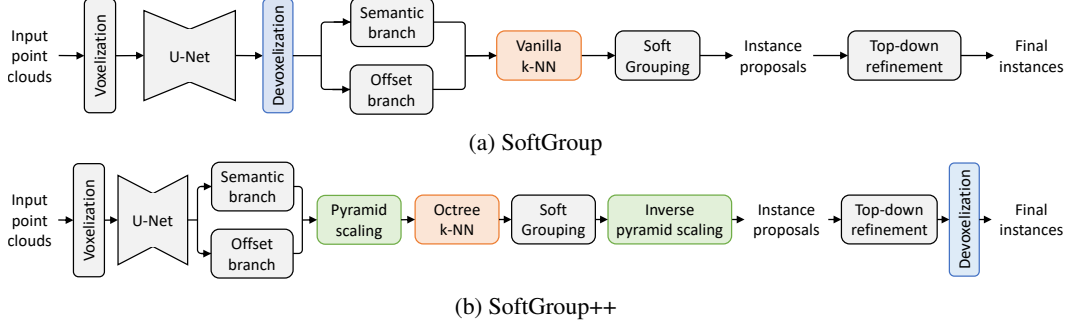


Figure 2: Architecture comparison between SoftGroup and SoftGroup++.

---

**Algorithm 1.** Pyramid scaling

---

**Input:**  $L$ : number of pyramid levels,  $V$ : base voxel size,  $C$ : number of classes,  
 $t = [t_1, \dots, t_L]$ : increasing order thresholds to determine pyramid levels.  
 $S$ : semantic predictions,  
 $O$ : offset predictions.  
**Output:**  $S'$ : semantic predictions after pyramid scaling,  
 $O'$ : offset predictions after pyramid scaling.

- 1 Initialize empty sets  $S' = \{\}$  and  $O' = \{\}$
- 2 **for**  $i = 1$  **to**  $C$  **do**
- 3     Extract semantic and offset prediction subsets for  $i$ -th class  $S_i \subset S$  and  $O_i \subset O$
- 4     Get number of voxels in the subset  $|S_i|$
- 5     Compute pyramid level:  $l = \operatorname{argmin}_{j \in \{1, \dots, L\}} \{t_j > |S_i|\}$
- 6     Voxelize  $S_i$  and  $O_i$  with voxel size being  $l \times V$  which results in  $S'_i$  and  $O'_i$
- 7     Aggregate downscaled results:  $S' = S' \cup S'_i$ ,  $O' = O' \cup O'_i$

---

below subsections, we present SoftGroup++. For the components that are similar to SoftGroup, we only briefly summarize the relevant details related to our method. We kindly refer readers to [37] for further details.

### 3.1 Point-wise Prediction Network

Point-wise prediction network, which composes of the backbone, semantic, and offset branches, receives point clouds as input to produce semantic and offset predictions. The input data is a set of points, each of which is represented by its 3D coordinates and features (such as RGB color). The model begins with a voxelization step, which produces a mapping and inverse mapping between point and voxel. Each voxel can be considered as the prototype of the points it covers. The coordinates and features of voxels are derived from the corresponding points by taking mean values. The voxelized input is fed into a U-Net style network to obtain backbone features. Here, differing from SoftGroup, the proposed SoftGroup++ directly uses backbone features as the input of semantic and offset branches without devoxelization.

### 3.2 Pyramid Scaling

The semantic and offset predictions are used as the input of octree  $k$ -NN and soft grouping. To reduce the search space for these components, we further downscale the semantic and offset predictions. Here, scaling is implemented by voxelization. A naive scaling strategy is to directly voxelize (*i.e.*, downsample) the predictions of the whole scene with a single voxel size (*i.e.*, downscale factor). However, this strategy exhibits limitations: (1) it is difficult to choose a fixed voxel size for downsampling the whole scene since different object classes may have different object sizes, and (2) the dissension of the prediction scores in local regions may lead to noise in the outputs since voxelization requires score averaging. As shown in our experiment section, this strategy severely worsens the prediction accuracy. We propose pyramid scaling to address these limitations. The key idea of pyramid scaling is to count the total number of points for each class in a scene and then

---

**Algorithm 2.** Octree  $k$ -NN

---

**Input:**  $q$ : point query,  $r$ : search radius,

$S(q, r)$ : sphere with center  $q$  and radius  $r$ ,

$root$ : root node of constructed octree, each node is associated with corresponding box, points, and octants.

**Output:** top  $k$  nearest neighbors w.r.t. query  $q$  and radius  $r$ .

```
1 Initialize an empty point list  $P$ 
2 Initialize an empty node queue  $Q$ 
3  $Q.enqueue(root)$ 
4 while  $Q$  is not empty do
5      $node = Q.dequeue()$ 
6     if  $node.box \cap S(q, r) \neq \emptyset$  then
7         if  $node$  is not leaf then
8             for  $octant$  in  $node.octants$  do
9                  $Q.enqueue(octant)$ 
10        else
11             $P.append(node.points)$ 
12 Perform  $k$ -NN of query  $q$  with radius search  $r$  on point set  $P$ 
```

---

determine the corresponding downscale factor. Furthermore, since downscaling is performed in a class-wise manner, prediction scores in local regions share similarities, thus reducing noise in the downscaled outputs.

The details of pyramid scaling are presented in Algorithm 1. The algorithm iterates through  $C$  classes and extract semantic  $S_i$  and offset  $O_i$  subsets for  $i$ -th class. The pyramid level  $l$  is computed by comparing the number of points in  $S_i$  and predefined thresholds  $t$ . Then,  $S_i$  and  $O_i$  are downscaled with a voxel size of  $l \times V$ , where  $V$  is the base voxel size. The downscaled semantic and offset predictions of all classes are aggregated and used as the input for the next component of the proposed method. We also save all the voxelization inverse maps in line #6 of Algorithm 1 to perform inverse pyramid scaling later.

### 3.3 Octree $k$ -NN

In recent grouping-based instance segmentation methods [13, 5, 37],  $k$ -NN serves as the prerequisite for grouping that constructs the point adjacency matrix. To cope with varying point density, a radius constraint  $r$  is added such that the distance from a valid neighbor to the query point should be less than  $r$ . Existing methods adopt vanilla  $k$ -NN algorithm, where pair-wise distance needs to be evaluated on the whole point set, and thus the time complexity of this algorithm w.r.t. the number of points is  $\mathcal{O}(n^2)$ . Since this quadratic time complexity is not scalable, we propose octree  $k$ -NN with a time complexity of  $\mathcal{O}(n \log n)$ .

**Constructing Octree.** Octree is a data structure that partitions the 3D space by recursively subdividing it into eight octants. Given a set of points, we first derive its tight axis-aligned bounding box. Then we recursively divide the 3D box into eight child boxes (octants). To balance the construction and traversal time, we limit the number of tree levels  $M$  to a small value (*e.g.*, 3) and store points in the last tree level (leaf nodes).

**$k$ -Nearest Neighbor Search on Octree.** Given query point  $q$  and the constructed octree, we are ready to perform  $k$ -NN of the query  $q$  with radius search  $r$ . The details are presented in Algorithm 2. The core idea of the algorithm is to find a small point subset near the query and then perform vanilla  $k$ -NN on the subset as opposed to the whole set. Starting from the root node, the algorithm recursively traverses through the tree. If the box associated with the current node intersects the sphere  $S(q, r)$ , there exist octants of the current node that intersects the sphere  $S(q, r)$ . These octants are enqueued and then checked in next iterations. The procedure is repeated until the leaf nodes. A point list  $P$  is used to store all the points associated with the leaf nodes having intersections with the sphere  $S(q, r)$ . Figure 3a illustrates the results of the algorithm on a two-level tree. For a neat presentation,

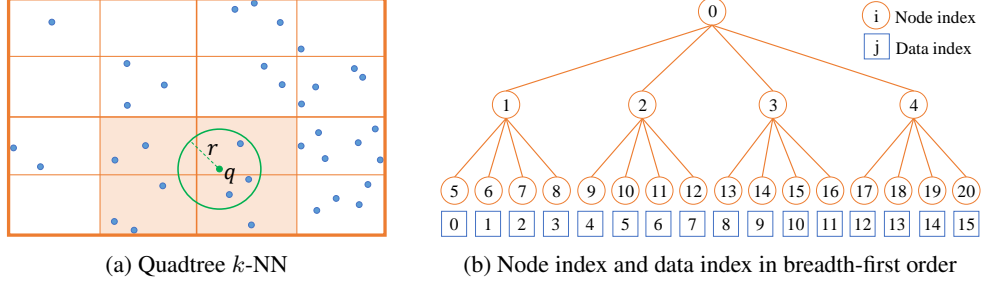


Figure 3: **Visualization of quadtree  $k$ -NN and breadth-first indices.** For neat presentation, we consider a quadtree of 2D data. (a) **Illustration of 2-level quadtree  $k$ -NN on query  $q$  with search radius  $r$ .** There are 4 leaf nodes (highlighted in orange background) that intersects query circle. Quadtree  $k$ -NN only measures distance from query to the points in these leaf nodes instead of the whole point set. (b) **Illustration of node and data indices in breadth-first order.** From breadth-first order, the recursive structure of the tree can be unfolded where child nodes and data indices can be retrieved by simple arithmetic given in Eqs. 1 and 2 such that the tree-based search algorithm can be parallelized effectively on GPU.

we consider a quadtree which is the 2D version of the octree. The query sphere has intersections with 4 boxes of leaf nodes, of which the points are taken to perform  $k$ -NN with the query.

To construct the adjacency matrix of all points, the algorithm is performed on each point of the point set, which requires GPU parallelization for a speed boost. One of the main challenges for parallelization is that the implementation of recursive tree traversal on CUDA kernel is nontrivial. Inspired by [25, 29], we present a simple strategy to unfold and traverse the tree using direct indexing, such that the algorithm is performed on each CUDA kernel for each point effectively. To this end, when constructing the tree, we index the tree nodes in breadth-first order, as shown in Figure 3b, given a parent node index  $i$ , we can access its child nodes directly by simple arithmetic:

$$\text{ch}_j(i) = i \times 2^d + j \text{ for } j = 1..2^d \quad (1)$$

where  $\text{ch}_j(i)$  is index of the  $j$ -th child node and  $d$  is dimension ( $d$  is 3 in octree or 2 in quadtree). Differ from [25, 29], we construct a full tree such that it is not required to encode the tree structure. The data index to access the points associated with the leaf node  $i$  can be simply derived as:

$$\text{data}(i) = i - \sum_{j=0}^{M-1} 2^{jd} \quad (2)$$

Since node and data indices are derived via simple arithmetic, we can unfold the recursive structure and parallelize the octree  $k$ -NN such that each CUDA kernel performs the algorithm for a query.

### 3.4 Instance Proposal Generation

After constructing the point adjacency matrix, we are ready to generate instance proposals. We adopt the soft grouping module of [37]. We traverse through the graph represented by the point adjacency matrix and then group the points having links into instance proposals. It is noted that the instance proposals have different scales due to pyramid scaling. We perform inverse pyramid scaling to make all instance proposals have the same scale. To this end, inverse mappings of the voxelization step (in Section 3.2) are used to perform inverse scaling.

### 3.5 Top-Down Refinement and Late Devoxelization

The instance proposals are refined by predicting the instance mask, classification score, and Intersection over Union (IoU) score. The refined proposals are devoxelized to obtain final instances. Here, we perform late devoxelization such that the devoxelization is delayed towards the end of the network, thus ensuring low computational cost for intermediate network components.

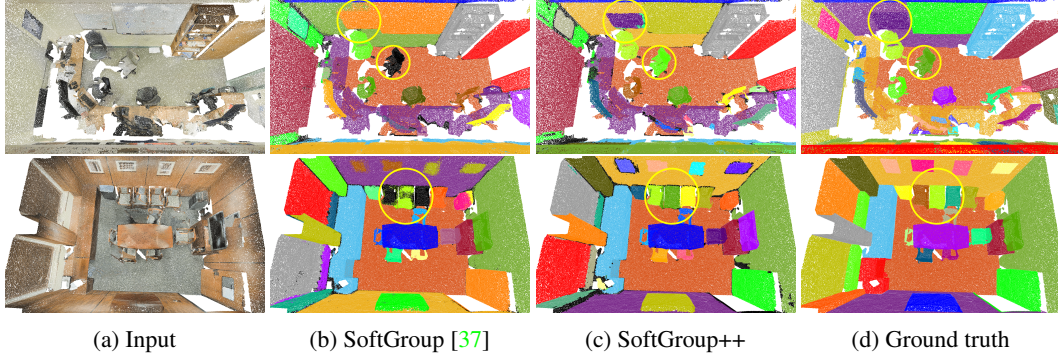


Figure 4: Qualitative results on S3DIS dataset. Predicted instances are illustrated in different random colors except for background which is in black. Visualization comparison is highlighted by yellow circles. Some instances are not separated or misdetected by SoftGroup. SoftGroup++ produces more accurate segmentation results. **Zoom in for best view.**

## 4 Experiments

### 4.1 Experimental Settings

**Datasets.** The experiments are conducted on various indoor and outdoor datasets, including S3DIS [1], ScanNet v2 [8], STPLS3D [4]. We provide dataset details in the supplementary.

**Evaluation Metrics.** The evaluation metrics are average precision and runtime. Regarding average precision,  $AP_{50}$  and  $AP_{25}$  denote the scores with IoU thresholds of 50% and 25%, respectively. Likewise, AP denotes the averaged scores with IoU threshold from 50% to 95% with a step size of 5%. For a fair runtime comparison, we attempt to measure the existing methods from released code on the same RTX 8000.

Table 1: Benchmarking results on S3DIS dataset. Methods marked with  $\dagger$  are evaluated on Area 5, and methods marked with  $\ddagger$  are evaluated on 6-fold cross validation.

Method	AP	$AP_{50}$	$mPrec_{50}$	$mRec_{50}$	Time (s)
SGPN $^\dagger$ [38]	-	-	36	28.7	-
ASIS $^\dagger$ [39]	-	-	55.3	42.4	-
PointGroup $^\dagger$ [13]	-	57.8	61.9	62.1	-
SSTNet $^\dagger$ [20]	42.7	59.3	65.5	64.2	-
HAIS $^\dagger$ [5]	-	-	71.1	65.0	4.09
SoftGroup $^\dagger$ [37]	<b>51.6</b>	66.1	73.6	66.6	2.46
<b>SoftGroup++<math>^\dagger</math></b>	50.9	<b>67.8</b>	<b>73.8</b>	<b>67.6</b>	<b>0.39</b>
SGPN $^\ddagger$ [38]	-	-	38.2	31.2	-
ASIS $^\ddagger$ [39]	-	-	63.6	47.5	-
3D-BoNet $^\ddagger$ [44]	-	-	65.6	47.7	8.02
PointGroup $^\ddagger$ [13]	-	64.0	69.6	69.2	-
SSTNet $^\ddagger$ [20]	54.1	67.8	73.5	73.4	-
HAIS $^\ddagger$ [5]	-	-	73.2	69.4	3.87
SoftGroup $^\ddagger$ [37]	54.4	68.9	75.3	69.8	2.20
<b>SoftGroup++<math>^\ddagger</math></b>	<b>56.6</b>	<b>71.3</b>	<b>75.9</b>	<b>74.4</b>	<b>0.38</b>

**Implementation Details.** We strictly follow the implementation details of SoftGroup [37]. Unless otherwise specified, the default settings of the experiments are as follows. Pyramid scaling uses 3 levels with the threshold to determine pyramid level being  $t = [10^5, 10^6, +\infty]$ . The pyramid base voxel size is set to 0.02m, which equals the input voxel size. The search radius of octree  $k$ -NN is set to 0.04m. The number of octree levels is set to 3. The model is trained on 4 GPUs with a batch size of 16 (4 samples per GPU) using Adam optimizer [15]. The learning rate is initialized to 0.004 and scheduled by a cosine annealing [23].

Especially, the outdoor STPLS3D dataset [4] has sparse point density and large variance in number of points for each objects. Following [4], the base voxel size and search radius are increased to 0.33m and 0.9m, respectively. We also adjust pyramid thresholds to  $t = [10^4, 10^5, +\infty]$ .

### 4.2 Benchmarking Results

**S3DIS.** Table 1 benchmarks the performance and runtime of SoftGroup++ and recent state-of-the-art methods on S3DIS dataset [1]. The results show that the proposed method achieves superior performance and speed compared to the others. Regarding results on Area 5 of S3DIS, SoftGroup++ runs at 0.39s per scan which is nearly  $6\times$  faster than the second-best. SoftGroup++ also achieves improvements in terms of  $AP_{50}$ ,  $mPrec_{50}$ , and  $mRec_{50}$ . Regarding cross-validation results, a similar



runtime improvement of SoftGroup++ is shown. Notably, our method outperforms the second-best in terms of AP and AP<sub>50</sub> by 2.2% and 2.4%, respectively. This improvement highlights the impact of processing the whole scan in a single forward without dividing the input and merging the predicted results.

**ScanNet v2.** To demonstrate the generalization of the proposed method, we report the results on ScanNet v2 dataset [8]. Compared to S3DIS, ScanNet v2 has lower point density and much smaller number of points per scan. SoftGroup++ achieves the best AP<sub>50</sub> on both validation and hidden test sets. Regarding runtime, we also report the results on Titan X, which is commonly used in previous methods. SoftGroup++ runs at 0.2s and 0.14s on Titan X and RTX 8000, leading to 30% speed boost compared to the second-best.

Table 2: Benchmarking results on ScanNet v2 dataset. Numbers marked with \* are cited runtimes.

Method	AP <sub>50</sub>		Inference time (s)	
	Test	Val	Titan X	RTX 8000
GSPN [45]	14.3	37.8	12.70*	-
OccuSeg [10]	67.2	60.7	1.90*	-
PointGroup [13]	63.6	56.9	0.45	0.30
SSTNet [20]	69.8	64.3	0.43	0.29
HAIS [5]	69.9	64.1	0.34	0.27
SoftGroup [37]	76.1	67.6	0.29	0.20
<b>SoftGroup++</b>	<b>76.9</b>	<b>67.9</b>	<b>0.20</b>	<b>0.14</b>

**STPLS3D.** We additionally report the results of SoftGroup++ on STPLS3D and compare with the reported performance of PointGroup [13] and HAIS [5] in [4]. With identical training settings to those described in [4], SoftGroup++ significantly outperforms the second best in terms of AP/AP<sub>50</sub>/AP<sub>25</sub> by 2.1/7.8/11.2(%) while being nearly 2.5× faster. The significant performance and speed improvement on different indoor and outdoor datasets demonstrates the superiority and generalization of the proposed method.

Table 3: Benchmarking results on STPLS3D dataset.

Method	AP	AP <sub>50</sub>	AP <sub>25</sub>	Time (s)
PointGroup [13]	27.4	44.2	54.2	-
HAIS [5]	40.4	51.9	57.3	2.83
<b>SoftGroup++</b>	<b>42.5</b>	<b>59.7</b>	<b>68.7</b>	<b>1.17</b>

### 4.3 Qualitative Analysis

Figure 4 shows the visualization comparison between SoftGroup and SoftGroup++ on S3DIS dataset. As highlighted by yellow circles, some instances are not separated or misdetected by SoftGroup. We hypothesize that this problem stems from the negative impact of divide-and-merge strategy. SoftGroup++ processes the whole scene in a single forward with better contextual information, leading to more accurate segmentation results.

### 4.4 Ablation study

**Component-wise Analysis.** We report the experimental results of SoftGroup++ when different components are omitted. Table 5 shows the ablation results. Without proposed components, the runtime of the baseline model is 30.32s with  $k$ -NN being the computational bottleneck of 23.32s. When pyramid scaling, octree  $k$ -NN, and late devoxelization are individually applied, the runtime of the above bottleneck significantly to 1.32s, 2.82s, and 0.96s, respectively. When all proposed components are applied, the model achieves the lowest latency of 1.28s, which is nearly 24× faster than the baseline.

Table 4: Ablation study on pyramid scaling.

Approach	AP	AP <sub>50</sub>	AP <sub>25</sub>	Time (s)
Naive scaling	47.0	64.7	73.7	0.44
Pyramid scaling	<b>50.9</b>	<b>67.8</b>	<b>76.9</b>	<b>0.39</b>

**Effectiveness on Pyramid Scaling.** We compare the proposed pyramid scaling with the naive scaling strategy presented in subsection 3.2. Table 4 shows the comparison results. While running slightly faster, pyramid scaling achieves AP/AP<sub>50</sub>/AP<sub>25</sub> of 50.9/67.8/76.9(%) which is 3.9/3.1/3.2(%) improvement compared to naive scaling. The qualitative comparison between the two strategies is shown in Figure 5. As expected, naive scaling misclassifies the points at the object edges as the background (illustrated in black points), while the proposed pyramid scaling produces more accurate instance masks.



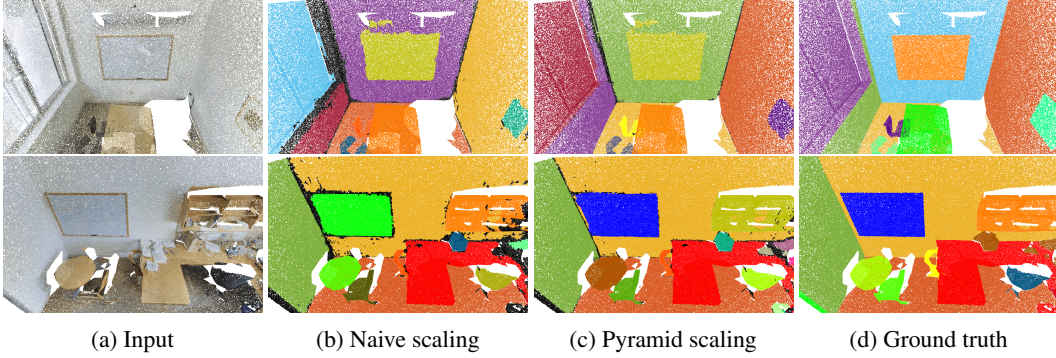


Figure 5: Qualitative comparison between naive scaling and the proposed pyramid scaling. Naive scaling misdetects the instance masks around object edges, which is illustrated in black points. The proposed pyramid scaling produces more accurate instance masks. **Zoom in for best view.**

Table 5: Ablation study on each component of the proposed method on the largest scene of Area 5 with  $\sim 4.5\text{M}$  points. The module-wise and total runtimes (in seconds) are measured on RTX 8000.

Baseline	Pyramid scaling	Octree	Late devoxel.	Point-wise	$k$ -NN	Grouping	Top-down	Total
✓				0.13	23.32	4.54	2.33	30.32
✓	✓			0.13	1.32	0.11	2.38	3.94
✓		✓		0.13	2.82	4.54	2.36	9.85
✓			✓	0.13	0.96	0.45	0.51	2.05
✓	✓	✓		0.13	1.28	0.11	2.35	3.87
✓	✓	✓	✓	0.13	0.44	0.23	0.48	<b>1.28</b>

**Octree  $k$ -NN.** We compare the running time between vanilla and octree  $k$ -NN when varying the number of points in Figure 6. The results show that the vanilla  $k$ -NN runtime grows quickly, while the octree  $k$ -NN runtime slightly increases.

#### 4.5 Limitations

SoftGroup++ is a bottom-up grouping-based method that performs grouping on learned point-wise predictions. The main limitation of SoftGroup is that the pyramid scaling is only able to consider class-wise manner, not instance-wise manner. This leads to negative impacts in scenes with many small objects of the same class. For instance, the downsample factor for chairs will be higher in the scene with hundreds of chairs compared to the scenes with a few chairs. This limitation can be addressed by estimating the number of objects for each class in the scene. However, this is outside the scope of this paper and we leave it for future research.

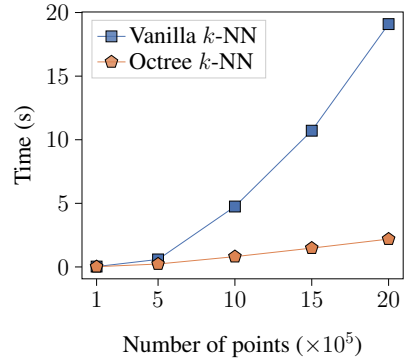


Figure 6: Ablation study on octree  $k$ -NN.

## 5 Conclusion

We have presented SoftGroup++ for scalable 3D instance segmentation on point clouds. SoftGroup++ address the computational bottleneck of SoftGroup with three important components, including octree  $k$ -NN, pyramid scaling, and late devoxelization. Notably, SoftGroup++ processes large scenes with millions of points by a single forward without dividing the input into multiple parts, avoiding limitations stemming from the divide-and-merge strategy. Experiments on various indoor and outdoor datasets demonstrate the superiority and generality of our method.

## References

- [1] Iro Armeni, Ozan Sener, Amir R Zamir, Helen Jiang, Ioannis Brilakis, Martin Fischer, and Silvio Savarese. 3d semantic parsing of large-scale indoor spaces. In *CVPR*, 2016. 2, 7
- [2] Mathieu Aubry, Ulrich Schlickewei, and Daniel Cremers. The wave kernel signature: A quantum mechanical approach to shape analysis. In *ICCV workshops*, 2011. 2
- [3] Michael M Bronstein and Iasonas Kokkinos. Scale-invariant heat kernel signatures for non-rigid shape recognition. In *CVPR*, 2010. 2
- [4] Meida Chen, Qingyong Hu, Thomas Hugues, Andrew Feng, Yu Hou, Kyle McCullough, and Lucio Soibelman. Stpls3d: A large-scale synthetic and real aerial photogrammetry 3d point cloud dataset. *arXiv:2203.09065*, 2022. 7, 8
- [5] Shaoyu Chen, Jiemin Fang, Qian Zhang, Wenyu Liu, and Xinggang Wang. Hierarchical aggregation for 3d instance segmentation. In *ICCV*, 2021. 1, 2, 3, 5, 7, 8
- [6] Xiaozhi Chen, Huimin Ma, Ji Wan, Bo Li, and Tian Xia. Multi-view 3d object detection network for autonomous driving. In *CVPR*, 2017. 1
- [7] Christopher Choy, JunYoung Gwak, and Silvio Savarese. 4d spatio-temporal convnets: Minkowski convolutional neural networks. In *CVPR*, 2019. 3
- [8] Angela Dai, Angel X Chang, Manolis Savva, Maciej Halber, Thomas Funkhouser, and Matthias Nießner. Scannet: Richly-annotated 3d reconstructions of indoor scenes. In *CVPR*, 2017. 7, 8
- [9] Benjamin Graham, Martin Engelcke, and Laurens Van Der Maaten. 3d semantic segmentation with submanifold sparse convolutional networks. In *CVPR*, 2018. 3
- [10] Lei Han, Tian Zheng, Lan Xu, and Lu Fang. Occuseg: Occupancy-aware 3d instance segmentation. In *CVPR*, 2020. 3, 8
- [11] Ji Hou, Angela Dai, and Matthias Nießner. 3d-sis: 3d semantic instance segmentation of rgb-d scans. In *CVPR*, 2019. 3
- [12] Binh-Son Hua, Minh-Khoi Tran, and Sai-Kit Yeung. Pointwise convolutional neural networks. In *CVPR*, 2018. 3
- [13] Li Jiang, Hengshuang Zhao, Shaoshuai Shi, Shu Liu, Chi-Wing Fu, and Jiaya Jia. Pointgroup: Dual-set point grouping for 3d instance segmentation. In *CVPR*, 2020. 1, 3, 5, 7, 8
- [14] David Inkyu Kim and Gaurav S Sukhatme. Semantic labeling of 3d point clouds with object affordance for robot manipulation. In *ICRA*, 2014. 1
- [15] Diederik P Kingma and Jimmy Ba. Adam: A method for stochastic optimization. In *ICVL*, 2015. 7
- [16] Jean Lahoud, Bernard Ghanem, Marc Pollefeys, and Martin R Oswald. 3d instance segmentation via multi-task metric learning. In *ICCV*, 2019. 3
- [17] Xin Lai, Jianhui Liu, Li Jiang, Liwei Wang, Hengshuang Zhao, Shu Liu, Xiaojuan Qi, and Jiaya Jia. Stratified transformer for 3d point cloud segmentation. In *CVPR*, 2022. 3
- [18] Juho Lee, Yoonho Lee, Jungtaek Kim, Adam Kosiorek, Seungjin Choi, and Yee Whye Teh. Set transformer: A framework for attention-based permutation-invariant neural networks. In *ICML*, 2019. 3
- [19] Yangyan Li, Rui Bu, Mingchao Sun, Wei Wu, Xinhan Di, and Baoquan Chen. Pointcnn: Convolution on x-transformed points. In *NIPS*, 2018. 3
- [20] Zhihao Liang, Zhihao Li, Songcen Xu, Minghui Tan, and Kui Jia. Instance segmentation in 3d scenes using semantic superpoint tree networks. In *ICCV*, 2021. 1, 3, 7, 8
- [21] Shih-Hung Liu, Shang-Yi Yu, Shao-Chi Wu, Hwann-Tzong Chen, and Tyng-Luh Liu. Learning gaussian instance segmentation in point clouds. *arXiv:2007.09860*, 2020. 1, 3
- [22] Yongcheng Liu, Bin Fan, Shiming Xiang, and Chunhong Pan. Relation-shape convolutional neural network for point cloud analysis. In *CVPR*, 2019. 3
- [23] Ilya Loshchilov and Frank Hutter. Sgdr: Stochastic gradient descent with warm restarts. In *ICVL*, 2017. 7

- [24] Daniel Maturana and Sebastian Scherer. Voxnet: A 3d convolutional neural network for real-time object recognition. In *IROS*, 2015. 3
- [25] Andrew Miller, Vishal Jain, and Joseph L Mundy. Real-time rendering and dynamic updating of 3-d volumetric data. In *GPGPU*, 2011. 6
- [26] Quang-Hieu Pham, Thanh Nguyen, Binh-Son Hua, Gemma Roig, and Sai-Kit Yeung. Jsis3d: joint semantic-instance segmentation of 3d point clouds with multi-task pointwise networks and multi-value conditional random fields. In *CVPR*, 2019. 1, 3
- [27] Charles R Qi, Hao Su, Kaichun Mo, and Leonidas J Guibas. Pointnet: Deep learning on point sets for 3d classification and segmentation. In *CVPR*, 2017. 2
- [28] Charles R Qi, Li Yi, Hao Su, and Leonidas J Guibas. Pointnet++: Deep hierarchical feature learning on point sets in a metric space. *arXiv:1706.02413*, 2017. 2
- [29] Gernot Riegler, Ali Osman Ulusoy, and Andreas Geiger. Octnet: Learning deep 3d representations at high resolutions. In *CVPR*, 2017. 3, 6
- [30] Olaf Ronneberger, Philipp Fischer, and Thomas Brox. U-net: Convolutional networks for biomedical image segmentation. In *MICCAI*, 2015. 3
- [31] Radu Bogdan Rusu, Nico Blodow, and Michael Beetz. Fast point feature histograms (fpfh) for 3d registration. In *ICVRA*, 2009. 2
- [32] Radu Bogdan Rusu, Nico Blodow, Zoltan Csaba Marton, and Michael Beetz. Aligning point cloud views using persistent feature histograms. In *IROS*, 2008. 2
- [33] Roni Permiana Saputra and Petar Kormushev. Casualty detection from 3d point cloud data for autonomous ground mobile rescue robots. In *SSRR*, 2018. 1
- [34] Yiru Shen, Chen Feng, Yaoqing Yang, and Dong Tian. Mining point cloud local structures by kernel correlation and graph pooling. In *CVPR*, 2018. 3
- [35] Martin Simonovsky and Nikos Komodakis. Dynamic edge-conditioned filters in convolutional neural networks on graphs. In *CVPR*, 2017. 3
- [36] Hugues Thomas, Charles R Qi, Jean-Emmanuel Deschaud, Beatriz Marcotegui, François Goulette, and Leonidas J Guibas. Kpconv: Flexible and deformable convolution for point clouds. In *ICCV*, 2019. 3
- [37] Thang Vu, Kookhoi Kim, Tung M Luu, Xuan Thanh Nguyen, and Chang D Yoo. Softgroup for 3d instance segmentation on point clouds. In *CVPR*, 2022. 1, 2, 3, 4, 5, 6, 7, 8
- [38] Weiyue Wang, Ronald Yu, Qiangui Huang, and Ulrich Neumann. Sgpn: Similarity group proposal network for 3d point cloud instance segmentation. In *CVPR*, 2018. 1, 3, 7
- [39] Xinlong Wang, Shu Liu, Xiaoyong Shen, Chunhua Shen, and Jiaya Jia. Associatively segmenting instances and semantics in point clouds. In *CVPR*, 2019. 1, 3, 7
- [40] Yue Wang, Yongbin Sun, Ziwei Liu, Sanjay E Sarma, Michael M Bronstein, and Justin M Solomon. Dynamic graph cnn for learning on point clouds. *ACM TOG*, 2019. 3
- [41] Yue Wang, Shusheng Zhang, Bile Wan, Weiping He, and Xiaoliang Bai. Point cloud and visual feature-based tracking method for an augmented reality-aided mechanical assembly system. *Int. J. Adv. Manuf. Technol.*, 2018. 1
- [42] Wenxuan Wu, Zhongang Qi, and Li Fuxin. Pointconv: Deep convolutional networks on 3d point clouds. In *CVPR*, 2019. 3
- [43] Yifan Xu, Tianqi Fan, Mingye Xu, Long Zeng, and Yu Qiao. Spidercnn: Deep learning on point sets with parameterized convolutional filters. In *ECCV*, 2018. 3
- [44] Bo Yang, Jianan Wang, Ronald Clark, Qingyong Hu, Sen Wang, Andrew Markham, and Niki Trigoni. Learning object bounding boxes for 3d instance segmentation on point clouds. In *NeurIPS*, 2019. 1, 2, 3, 7
- [45] Li Yi, Wang Zhao, He Wang, Minhyuk Sung, and Leonidas J Guibas. Gspn: Generative shape proposal network for 3d instance segmentation in point cloud. In *CVPR*, 2019. 3, 8
- [46] Hengshuang Zhao, Li Jiang, Jiaya Jia, Philip HS Torr, and Vladlen Koltun. Point transformer. In *ICCV*, 2021. 3
- [47] Jon Zubizarreta, Iker Aguinaga, and Aiert Amundarain. A framework for augmented reality guidance in industry. *Int. J. Adv. Manuf. Technol.*, 2019. 1